Modulated Model Predictive Control for Multilevel Cascaded H-Bridge Converter-Based Static Synchronous Compensator

Xiao, Qian; Jin, Yu; Jia, Hongjie; Mu, Yunfei; Ji, Yanchao; Teodorescu, Remus; Blaabjerg, Frede

Published in:
IEEE Transactions on Industrial Electronics

DOI (link to publication from Publisher):
10.1109/TIE.2021.3056953

Publication date:
2022

Document Version
Accepted author manuscript, peer reviewed version

Modulated Model Predictive Control for Multilevel Cascaded H-Bridge Converter based STATCOM

Qian Xiao, *Member*, *IEEE*, Yu Jin, Hongjie Jia, *Senior Member*, *IEEE*, Yunfei Mu, *Member*, *IEEE*, Yanchao Ji, Remus Teodorescu, *Fellow*, *IEEE*, Frede Blaabjerg, *Fellow*, *IEEE*

***Abstract*—The model predictive control (MPC) methods have been widely applied due to the fast dynamic performance and multiple control targets. However, they show certain limits when applied to the multilevel converters, such as unfixed switching frequency, large computation burden, and complex weighting factors selection. This paper proposes a novel modulated model predictive control (M^2PC) method for cascaded H-bridge (CHB) converter based static synchronous compensator (STATCOM). Instead of multi-targets integration and weighting factors design, the proposed method disintegrates the voltage balancing control process from the cost function. The evaluated control sets for output current control is decided by the search step and the search range in each period. By proper design and selection of the adaptive search step for the output voltage references under *α-β* coordinate, the search range can be reduced, which greatly reduces the number of evaluated control sets in each control period. Therefore, the dynamic of output characteristics and the low prediction computation burden of the MPC method are guaranteed simultaneously. In addition, with the simple and independent integration of the capacitor voltage balancing control, the proposed method can be easily applied in the CHB converter based STATCOM application. Furthermore, this paper provides a delay compensation for the prediction process, and it provides a fixed switching frequency for each H-bridge cell. Simulation and experimental results verify the effectiveness of the proposed M^2PC method.**

***Index Terms*—model predictive control (MPC), multilevel converter, cascaded H-bridge (CHB), static synchronous compensator (STATCOM), switching frequency.**

I. INTRODUCTION

Nowadays, multilevel converters have been widely applied in various medium-voltage (MV) and high power applications [1], [2]. Among them, the cascaded H-bridge (CHB) converter is considered to be one of the most attractive topologies in the MV static synchronous compensator (STATCOM) applications due to its excellent modularity, low economic cost [3], and fault-tolerant ability [4].

For the CHB converter based STATCOM, the linear controllers are usually applied due to its simple structure and easily manipulated robustness [5]. However, the multilayer linear control structures show limited performance on the dynamic response [6]. Therefore, much research has been carried out about nonlinear controllers [7]-[9]. Recently, model predictive control (MPC) technology has attracted much research interest in the power electronics field. The advantages of the MPC, such as fast dynamic responses, multiple control targets, and simple control structure, suits the nonlinear power electronics converters [10] perfectly.

Instead of exploring the close-loop control law, the MPC methods usually transform the controlled system into an online optimization problem, based on the derived discrete mathematical models and the corresponding cost functions about the control targets [11]. However, the conventional switching status based control sets in the finite control set (FCS) MPC methods [12] are unsuitable for the CHB converters due to the huge quantity of the evaluated control sets [13]. Therefore, much MPC research for CHB based converter focuses on the computation burden reduction. Considering the fact that each H-bridge cell in the CHB converter can generate three voltage levels, instead of the switching status, the output voltage level in each cell is used to predict the output current [14]. This method has been verified in CHB based inverter applications, and the computation burden is thus reduced. *P. Cortes et al.* proposes a space vector based MPC method for the CHB inverter, where only the vectors adjacent to the previous optimal one are evaluated in each period [15]. However, the complicated switching status selection for space vectors and the limited performance under huge power step constrain the further application of this method. With *Clark* transformation, the sphere-decoding algorithm based MPC method under *α-β* coordinate is proposed in [16] to reduce the computation burden by the multistep finite control set (FCS)-MPC method. The above MPC methods are suitable for CHB based inverter applications. For the CHB based STATCOM applications where there is no DC power supply in each cell, further exploration needs to be carried to control the capacitor voltages in each cell.

A cell-by-cell MPC method for a single-phase CHB rectifier is proposed in [17]. The predictive controller is applied in each cell to control both the output current and the capacitor voltages. However, it requires a large amount of calculation. To improve the capacitor voltage balancing ability and reduce the computation burden, the deadbeat control method is applied for the output current control, and the MPC method is applied to regulate the capacitor voltage by controlling the output voltage in each cell [18]. In [19], a multi-stages multi-objects FCS-MPC method is further proposed for the three-phase CHB based STATCOM. In this

This work was supported in part by the China Postdoctoral Science Foundation (Grant No. 2020TQ0222), and in part by the project of the National Natural Science Foundation of China (Grant No. 51625702, and 52061635103). (*Corresponding author: Yu Jin*).

Q. Xiao, H. Jia, and Y. Mu are with the Key Laboratory of Smart Grid of Ministry of Education, Tianjin University, Tianjin 300072, China, and also with the Key Laboratory of Smart Energy & Information Technology of Tianjin Municipality, Tianjin 300072, China (e-mail: xiaoqian@tju.edu.cn; hjjia@tju.edu.cn; yunfeimu@tju.edu.cn).

Y. Jin and Y. Ji is with the Department of Electrical Engineering and Automation, Harbin Institute of Technology, Harbin 150001, China. (email: hitjy19940213@163.com, hitjyc2016@163.com).

R. Teodorescu and F. Blaabjerg are with the Department of Energy Technology, Aalborg University, 9220 Aalborg, Denmark. (email: ret@et.aau.dk, fbl@et.aau.dk).

method, the first stage calculates the output voltage levels in each phase, and the second stage tries to regulate the capacitor voltage balancing. However, the cluster voltage balancing is integrated with individual capacitor voltage balancing in the cost function, which limits the phase leg balancing effect. Similar multi-stage FCS-MPC method [20] and improved corresponding priority sorting based approach [21] have also been applied in multilevel converters, simultaneously regulating the output current and the capacitor voltages. Based on these FCS-MPC methods, a simplified branch and bound approach for the multi-stage MPC method is proposed in [22]. With the transformation in the α-β frame, the computation burden of the current predictive control has been reduced. Furthermore, an improved parallel implementation method has been realized in [23]. By the parallel computation in DSP and FPGA, the execution time has been reduced greatly. However, the total calculation amount remains the same as the method in [22]. In addition, a novel *Diophantine* equations based predictive control is proposed in [24]. This FCS-MPC method replaces the time-consuming optimization algorithm by solving *Diophantine* equations over a large set of switching combinations. The execution time is reduced, but these FCS-MPC methods still have an unfixed switching frequency in each cell.

A modulated model predictive control (M^2PC) method is proposed for a double-star modular multilevel converter (DS-MMC) based voltage source converter in [25]. This method controls the duty cycle, rather than the switching process or the output voltage levels presented in other FCS-MPC methods. Other similar M^2PC methods for CHB converter based power electronics transformer (PET) [26] and CHB based back-to-back (BTB) converter [27] are realized by selecting two different optimal vectors and calculating the duty cycle of the selected optimal vectors. The fixed equivalent switching frequencies in the output voltage levels are realized in these M^2PC methods. However, the sorting based capacitor voltage balancing method cannot guarantee fixed switching frequency in each cell, and the cell capacitor voltage balancing is not well discussed in the above two applications. To solve the voltage balancing problem, an improved space vector (SV) based M^2PC is proposed for CHB based STATCOM application [28]. The SV voltage references are decided by similar steps under the α-β coordinate, and the voltage balancing between capacitors are realized by redundant switching states selection. However, the unfixed switching frequency in each cell remains in this method. Designed for the DS-MMC, a two-stage M^2PC method is proposed with carrier-phase-shift (CPS)-PWM [29]. This method considers the multilevel converter as a two-level converter. Then it calculates the duty cycle of the optimal vectors and applies them to CPS-PMW. However, the complicated optimal vectors selection and the corresponding duty cycle calculation still need to be improved for CHB converters in the STATCOM application.

In addition, the computation delay brought by the signal transmission and control system also needs to be compensated. Many recent research papers have been published about delay compensation, which can mainly be classified into two categories, indirect and direct compensation [30]. For the indirect compensation method, the time delay is mainly compensated by some other predictive methods such as deadbeat predictive control [31]. For the direct compensation method, they are usually realized in the MPC algorithm, which is also known as the two-step prediction method. In [32], the control references are predicted two-step ahead, and the new control references are compared to the predicted value in the next control period. Another widely applied direct delay compensation method is analyzed in [33], where the references and the output value two-step ahead are estimated and applied to realize delay compensation.

This paper proposes a novel modulated model predictive control (M^2PC) method, especially for CHB converter based STATCOM. The main characteristics of the proposed method are listed below.

1) The output voltage references are taken as the basic component in the control set, which is decided by the search step and search range in each period. By proper design of the adaptive search step, a fixed and reduced number of the control sets are evaluated in each period for the proposed method. The output characteristics in the CHB converter are guaranteed, and the computation burden of the model prediction process is greatly reduced.
2) By implementation of the M^2PC method under the α-β coordinate, the output current control is realized by output voltage references in the α and β axes, and the cluster DC voltage balancing is controlled by output voltage references in the *0* axis. Therefore, the output current and the cluster DC voltage balancing control is disintegrated, and the weighting factors design for the multi-targets in the cost function are eliminated.
3) The delays introduced by the signal transmission, control, and modulation process are considered, and the delay compensation method for the proposed M^2PC method is analyzed.
4) The proposed M^2PC method generates a fixed switching frequency in each cell by CPS-PWM, and the switching loss in each cell is thus more evenly distributed.

The rest of the paper is outlined as follows. Section II introduces the model and basic working principle of the CHB converter. The detailed principle of the proposed M^2PC method is introduced in Section III. Simulation results in Section IV and experimental results in Section V verify the effectiveness of the proposed method. The conclusions are listed in Section VI.

II. The System Model of the CHB Converter

The topology of the three-phase star-connected multilevel CHB converter based STATCOM is shown in Fig. 1. The CHB converter consists of three identical phase clusters, each of which includes N series-connected H-bridge cells. The output terminal of each cluster is connected to the AC grid through a filter inductor L. In each cell, there are four IGBT switches and one DC link capacitor. With the combination of the switching status, each cell can generate three voltage levels, +1, 0, and −1, where +1, 0, and −1 represent this cell outputting positive DC voltage, 0, and negative DC voltage. By control of the final output voltages in each phase cluster,

This article has been accepted for publication in a future issue of this journal, but has not been fully edited. Content may change prior to final publication. Citation information: DOI 10.1109/TIE.2021.3056953, IEEE Transactions on Industrial Electronics

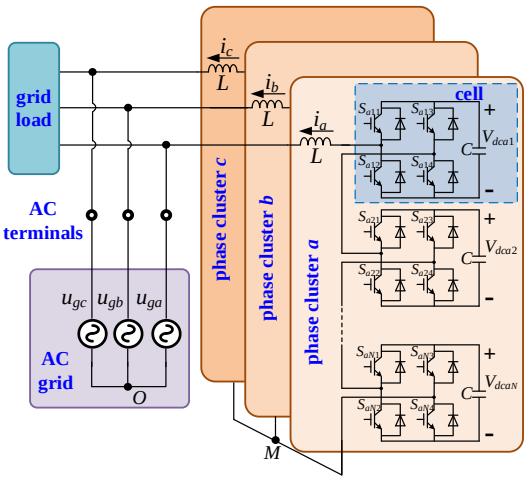

Fig. 1. The topology of the CHB converter based STATCOM.

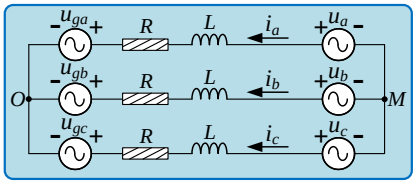

Fig. 2. The equivalent circuit of the CHB converter.

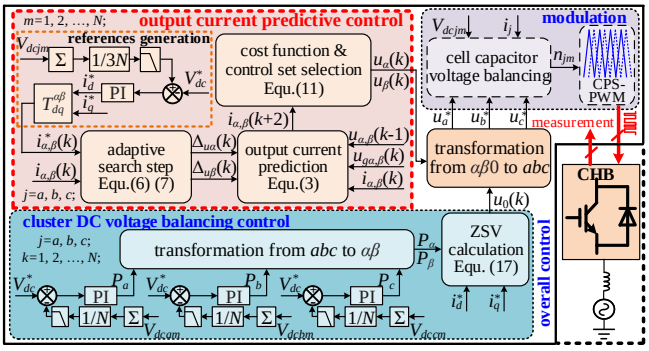

Fig. 3. The control block diagram of the proposed M2PC method.

the output current of the CHB converter can be controlled to realize reactive power compensation.

To analyze the system model of CHB converter, the equivalent circuit of the CHB converter is shown in Fig. 2, where R is the equivalent resistor of the filter inductor L. Applying the *Kirchhoff* voltage/current laws to the equivalent circuit in Fig. 2, the system model of the CHB converter based STATCOM can be expressed as

$$L\frac{d}{dt}\begin{bmatrix} i_a \\ i_b \\ i_c \end{bmatrix} = \begin{bmatrix} u_{ga} \\ u_{gb} \\ u_{gc} \end{bmatrix} - \begin{bmatrix} u_a \\ u_b \\ u_c \end{bmatrix} - R\begin{bmatrix} i_a \\ i_b \\ i_c \end{bmatrix} \tag{1}$$

where u_a, u_b, and u_c are the output voltages in the three phase clusters of the CHB converter.

By *Clark* transformation, the system model of the CHB converter based STATCOM can be further transferred into α-β coordinate as follows [23].

$$L\frac{d}{dt}\begin{bmatrix} i_\alpha \\ i_\beta \end{bmatrix} = \begin{bmatrix} u_{g\alpha} \\ u_{g\beta} \end{bmatrix} - \begin{bmatrix} u_\alpha \\ u_\beta \end{bmatrix} - R\begin{bmatrix} i_\alpha \\ i_\beta \end{bmatrix} \tag{2}$$

where i_α and i_β are the output current components in α and β axes; $u_{g\alpha}$ and $u_{g\beta}$ are the AC grid voltage components in α and β axes; u_α and u_β are the output voltage components in α and β axes.

The equation (2) can be further discretized using the forward *Euler* approximation. The final discrete system model of the CHB converter based STATCOM can be expressed as follows.

$$\begin{cases} i_\alpha(k+1) = \dfrac{T_s}{L}(u_{g\alpha}(k) - u_\alpha(k)) - (1 - \dfrac{T_s R}{L})i_\alpha(k) \\ i_\beta(k+1) = \dfrac{T_s}{L}(u_{g\beta}(k) - u_\beta(k)) - (1 - \dfrac{T_s R}{L})i_\beta(k) \end{cases} \tag{3}$$

where T_s is the sampling period; $i_\alpha(k+1)$ and $i_\beta(k+1)$ are the predicted output currents at $k+1$ time instant; $u_{g\alpha}(k)$ and $u_{g\beta}(k)$ are the measured grid voltages at k time instant; $u_\alpha(k)$ and $u_\beta(k)$ are the output voltage references at k time instant; $i_\alpha(k)$ and $i_\beta(k)$ are the measured output current at k time instant.

It can be seen that the output current in the next $k+1$ time instant is determined by the output current and the output voltage references in the current k time constant. With the above equations, the output current of the CHB converter can be predicted under different output voltage references.

It is noted that the zero-sequence component of the output voltages will not affect the output current of the CHB converter. Therefore, for the output voltage references, only the components in α and β axes are considered for the output current control. The zero-sequence voltage (ZSV) component will be used for the cluster DC voltage balancing control.

III. The Proposed M²PC Method for CHB STATCOM

A. The overall control diagram

In this paper, a novel M²PC method is proposed with a fixed switching frequency in each cell and a reduced computation burden. As shown in Fig. 3, the proposed M²PC method mainly includes three individual parts, the output current predictive control, the cluster DC voltage balancing control, and the modulation scheme.

The output current predictive control is applied to control the output current of the CHB converter based STATCOM. In this part, $i_{\alpha,\beta}^*(k)$ represents $i_\alpha^*(k)$ and $i_\beta^*(k)$, the measured output currents in the α and β axes at k time instant; $u_{\alpha,\beta}(k\text{-}1)$ represents $u_\alpha(k\text{-}1)$ and $u_\beta(k\text{-}1)$, the optimal control sets at the last k-1 time instant; $i_{\alpha,\beta}(k)$ represents $i_\alpha(k)$ and $i_\beta(k)$; $u_{\alpha,\beta}(k)$ represents $u_\alpha(k)$ and $u_\beta(k)$; represents $i_\alpha^*(k)$ and $i_\beta^*(k)$; $\Delta_{u\alpha}(k)$ and $\Delta_{u\beta}(k)$ are the adaptive search step in the α and β axes for the proposed algorithm; V_{dcjm} is measured capacitor voltage in each cell; V_{dc}^* is the DC capacitor voltage reference in each cell; $T_{\alpha\beta}^{dq}$ is the transfer matrix from the dq coordinate to the $\alpha\beta$ coordinate.

The cluster DC voltage balancing control is designed to control and balance the average cell capacitor voltages among the three phases. In this part, P_a, P_b, and P_c are the calculated active power in each phase to adjust the cluster DC voltage between the three phases; P_α and P_β are the transformed components in the $\alpha\beta$ coordinate;. i_d^* and i_q^* are the output current references in the dq coordinate; $u_0(k)$ is the final calculated ZSV used for cluster DC voltage balancing.

The CPS-PWM is applied in the modulation scheme, where a fixed switching frequency is obtained in each cell. n_{jm} is the final modulation reference of each cell. The modulation scheme mainly realizes the voltage references normalization

This article has been accepted for publication in a future issue of this journal, but has not been fully edited. Content may change prior to final publication. Citation information: DOI 10.1109/TIE.2021.3056953, IEEE Transactions on Industrial Electronics

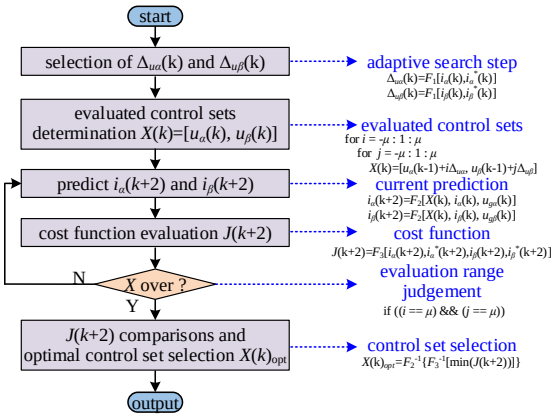

Fig. 4. The flowchart diagram of the proposed output current predictive control method.

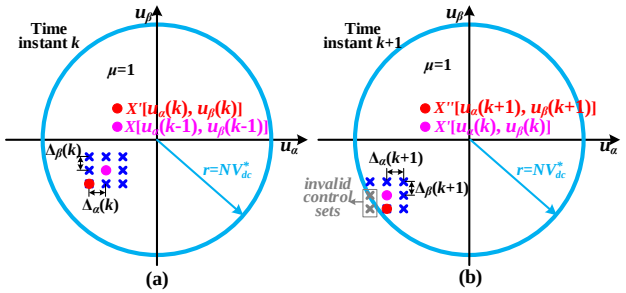

Fig. 5. The working principle of the proposed output current predictive control method. (a) The predictive control process at k time instant. (b) The predictive control process at k+1 time instant.

and the individual capacitor voltage balancing in each cell.

B. The output current predictive control

Before a detailed introduction, it is noted that output voltage references, $u_\alpha(k)$ and $u_\beta(k)$, are the basic component of the control set. Therefore, the evaluated control set in this paper can be expressed as

$$X(k)=\left[u_\alpha(k),\ u_\beta(k)\right] \tag{4}$$

1) *The basic flowchart of the current predictive control*

The basic flowchart of the proposed M^{2}PC method is shown in Fig. 4. Firstly, the adaptive search step $\Delta_{u\alpha}$ and $\Delta_{u\beta}$ are calculated according to the difference between the output current references and their measured values. Then, the evaluated control sets for the current k time instant are decided based on $\Delta_{u\alpha}$ and $\Delta_{u\beta}$. Next, the output currents under the selected control set are predicted, and the corresponding cost functions are calculated according to the discrete model and the measured state variables. Finally, the optimal control set is selected based on the calculated cost function.

2) *The adaptive search step and the evaluated control sets*

For the proposed M^{2}PC method, there are mainly two factors that affect the performance of the control method, the search range μ and the search step Δ ($\Delta_{u\alpha}$ and $\Delta_{u\beta}$).

With the determined μ, $\Delta_{u\alpha}$, and $\Delta_{u\beta}$, the evaluated control sets can be expressed as

$$\begin{aligned} &for\ i=-\mu:1:\mu \\ &\quad for\ j=-\mu:1:\mu \\ &\qquad X(k)=\left[u_\alpha(k-1)+i\Delta_{u\alpha}(k),\ u_\beta(k-1)+j\Delta_{u\beta}(k)\right] \end{aligned} \tag{5}$$

It is noted that to reduce the computation burden of the proposed method, the search range μ is selected as 1.

Normally, a larger search range μ increases the dynamics response of the proposed method, but it also increases the computation burden significantly. Correspondingly, a larger search step Δ also improves the dynamic response of the proposed method. However, at the same time, it also deteriorates the steady performance and increases the system oscillation around the steady-state operation point. Therefore, to obtain a fixed search range μ and reduced computation burden, the adaptive search step $\Delta_{u\alpha}$ and $\Delta_{u\beta}$ should be empirically tuned to obtain a suitable dynamic response together with a satisfying steady-state performance. More discussion about the influence of the search range μ, and the search step ($\Delta_{u\alpha}$ and $\Delta_{u\beta}$) can be found in the simulation part in Section IV.

With the determined search range μ, the adaptive search step $\Delta_{u\alpha}$ and $\Delta_{u\beta}$ can be designed as follows. When the error between the output currents and their references are big, the search step should increase to improve the dynamic response. When the error between the output currents and their references are small, the search step should decrease to reduce the system oscillation. Therefore, the adaptive search step can be selected based on the following principle

$$\begin{bmatrix}\Delta_{u\alpha}(k)\\ \Delta_{u\beta}(k)\end{bmatrix}=\frac{\varepsilon NV_{dc}^*}{I_{amp}(k)}\begin{bmatrix}|\,i_\alpha^*(k)-i_\alpha(k)\,|\\ |\,i_\beta^*(k)-i_\beta(k)\,|\end{bmatrix} \tag{6}$$

where I_{amp}(k) is the amplitude of the output current references at k time instant; N is the number of cells in each phase cluster; V_{dc}^* is the rated cell capacitor voltage in each cell; ε is the empirical parameter. In this paper, ε is selected as 1 in this paper.

In the meantime, there should be an upper limit and a lower limit to the search step. Therefore a saturation function is applied for the final value, which can be expressed as

$$Sat(\Delta)=\begin{cases}\Delta_{up\_lim}, & \Delta>\Delta_{up\_lim}\\ \Delta, & \Delta_{low\_lim}<\Delta<\Delta_{up\_lim}\\ \Delta_{low\_lim}, & \Delta<\Delta_{low\_lim}\end{cases} \tag{7}$$

where Δ represents the value of the search step $\Delta_{u\alpha}$ and $\Delta_{u\beta}$ in equation (7); Δ_{up_lim} and Δ_{low_lim} are selected as $0.2NV_{dc}^*$ and $0.005NV_{dc}^*$. A similar detailed parameter design principle for the adaptive search step can be found in [10]. It is also noted that the lower limit is designed to avoid oscillation. Whether it is necessary should be decided by the actual t requirement of the practical project.

After the determination of the adaptive search step, the final evaluated control sets can be selected as in equation (5). However, it should be noted that the effective control sets have to meet the following constraint

$$u_\alpha^{\,2}(k)+u_\beta^{\,2}(k)\le(NV_{dc}^*)^2 \tag{8}$$

A more detailed control sets selection process can be seen in Fig. 5, where the two components $u_\alpha(k)$ and $u_\beta(k)$ should be within the circle with a radius of NV_{dc}^*. Control sets beyond this circle are invalid and will not be considered in the predictive control process.

3) *The current prediction and cost function evaluation*

With the above design of the adaptive search step and the evaluated control sets, the output current can be predicted

This article has been accepted for publication in a future issue of this journal, but has not been fully edited. Content may change prior to final publication. Citation information: DOI 10.1109/TIE.2021.3056953, IEEE Transactions on Industrial Electronics

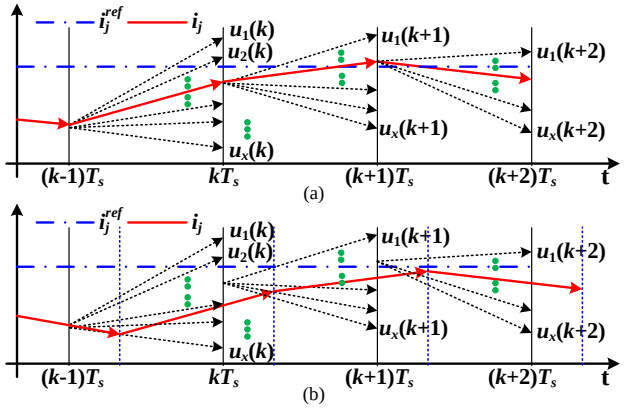

Fig. 6. Implement of MPC algorithm. (a) Ideal cases ignoring delay. (b) Practical cases with computation delay.

based on the discrete CHB converter model in equation (3).

The control target of the current predictive control only contains the output currents, and the cell voltage balancing will be realized in the cluster DC voltage balancing control and the modulation scheme. Therefore, the final cost function only includes the control target of output current in the α and β axes, which can be expressed as

$$J(k+1)=|i_\alpha^*(k+1)-i_\alpha(k+1)|+|i_\beta^*(k+1)-i_\beta(k+1)| \quad (9)$$

where $i_\alpha^*(k+1)$ and $i_\beta^*(k+1)$ are the output current references at k+1 time instant, which can be derived based on the *Lagrange* third-order extrapolation method [13]. They can be expressed as

$$\begin{cases} i_\alpha^*(k+1)=4i_\alpha^*(k)-6i_\alpha^*(k-1)+4i_\alpha^*(k-2)-i_\alpha^*(k-3) \\ i_\beta^*(k+1)=4i_\beta^*(k)-6i_\beta^*(k-1)+4i_\beta^*(k-2)-i_\beta^*(k-3) \end{cases} \quad (10)$$

where $i_\alpha^*(k)$, $i_\alpha^*(k\text{-}1)$, $i_\alpha^*(k\text{-}2)$, and $i_\alpha^*(k\text{-}3)$ are the output current references in the α axis at k, k-1, k-2, and k-3 time instant; $i_\beta^*(k)$, $i_\beta^*(k\text{-}1)$, $i_\beta^*(k\text{-}2)$, and $i_\beta^*(k\text{-}3)$ are the output current references in the β axis at k, k-1, k-2, and k-3 time instant.

Substituting (3) and (10) into (9), the final cost function under each control set can be evaluated. After calculating all the cost functions, the control set with the minimum cost function will be selected as the optimal control set for the next time instant.

Based on the above descriptions, the working principle of the proposed M^{2}PC method can be further presented in Fig. 5. Supposing the optimal control set at k-1 time instant is $X[u_\alpha(k\text{-}1), u_\beta(k\text{-}1)]$, the effective control sets adjacent to X are evaluated. To better track the output current references, the control set with the minimum J(k+1) is $[u_\alpha(k\text{-}1)\text{-}\Delta_{u\alpha}, u_\beta(k\text{-}1)\text{-}\Delta_{u\beta}]$, and it will be selected as the optimal control set $X'[u_\alpha(k), u_\beta(k)]$at k time instant. Then, at the time instant k+1, the effective control sets adjacent to X' are evaluated, and the control set with the minimum J(k+2) is $[u_\alpha(k), u_\beta(k)\text{-}\Delta_{u\beta}]$, and it will be selected as the optimal control set $X''[u_\alpha(k+1), u_\beta(k+1)]$at k+1 time instant.

C. Computation delay and delay compensation

In the practical field application, the system needs to sample and communicate a large amount of data and evaluate a large number of the control sets within each sampling period. Since the dynamic response of the realistic hardware system is fast, the computation delay can be significant compared to the desired closed-loop response. The comparison diagram between the ideal predictive control process and the actual predictive control process is shown in Fig. 6. As shown in Fig. 6 (a), when there is no computation delay, the selected control set at the k time instant will decide the output characteristic of the k time instant. However, in the actual control system in Fig. 6 (b), the computation delay will bring inevitable control error into the CHB based STATCOM system.

To solve this problem, this paper analyzes the delay compensation approach for the proposed M^{2}PC method. In this compensation approach, the control references at the k time instant are decided by the one evaluated at the k-1 time instant. Normally, the computation delay is within one sampling period. Therefore, with the above-mentioned two-step ahead prediction process, at the k time instant, the output characteristics at the k+2 time instant are evaluated, and the optimal control references are sent to the control system at the k+1 time instant. Therefore, the delay effect of the system will be eliminated from the control system.

More specifically, at the k time instant, the final cost function with delay compensation of the proposed M^{2}PC method can be expressed as

$$J(k+2)=|i_\alpha^*(k+2)-i_\alpha(k+2)|+|i_\beta^*(k+2)-i_\beta(k+2)| \quad (11)$$

where $i_\alpha(k+2)$ and $i_\beta(k+2)$ are the predicted value, calculated by system model in equation (3); $i_\alpha^*(k+2)$ and $i_\beta^*(k+2)$ can be predicted by *Lagrange* extrapolation method in equation (10).

The obtained output voltage references $u_\alpha(k)$, $u_\beta(k)$ will be the references for the k+1 time instant. Hence, the delay compensation of the proposed M^{2}PC method is realized.

D. The cluster DC voltage balancing control

The cluster DC voltage balancing control can be realized by ZSV injection, and the ZSV injection will not influence the output current of the CHB converter [4].

Supposing the output currents of the CHB converter are

$$\begin{bmatrix} i_a \\ i_b \\ i_c \end{bmatrix}=\begin{bmatrix} I\cos(\omega t+\varphi_i) \\ I\cos(\omega t+\varphi_i-2\pi/3) \\ I\cos(\omega t+\varphi_i+2\pi/3) \end{bmatrix} \quad (12)$$

where φ_i is the phase angle between the output current and the grid voltage; ωt is the phase angle of the grid voltage.

Supposing the injected ZSV used for cluster voltage balancing is

$$u_0=V_0\cos(wt+\delta_0) \quad (13)$$

where u_0 is the injected ZSV; V_0 is the amplitude of u_0; δ_0 is the phase angle between ZSV and the grid voltage.

Based on the derivations in [4], the power flow generated by the ZSV can be expressed as

$$\begin{bmatrix} P_a \\ P_b \\ P_c \end{bmatrix}=\frac{V_0 I}{2}\begin{bmatrix} \cos(\varphi_i-\delta_0) \\ \cos(\varphi_i-\delta_0-2\pi/3) \\ \cos(\varphi_i-\delta_0+2\pi/3) \end{bmatrix} \quad (14)$$

As is shown in equation (14), the ZSV will not influence the total active power in the CHB converter, and it only adjusts the active power flow among the three phases. With the *Clark* transformation, equation (14) can be simplified as

This article has been accepted for publication in a future issue of this journal, but has not been fully edited. Content may change prior to final publication. Citation information: DOI 10.1109/TIE.2021.3056953, IEEE Transactions on Industrial Electronics

TABLE I COMPARISON OF DIFFERENT MPC CONTROL METHODS

Methods \ Items		Three phases	Weighting factors	Coordinate	Computation burden	Cell switching frequency	Delay compensation	Voltage balancing ability for CHB	Applications
FCS-MPC	[14]	Yes	No	*a*, *b*, *c*	Low	Variable	No	No	CHB based inverter
	[15]	Yes	No	*α*, *β*	Medium	Variable	No	No	
	[16]	Yes	Yes	*α*, *β*	Medium	Variable	No	No	
	[17]	Single-phase	Yes	---------	High	Variable	Yes	Yes	CHB based rectifier
	[18]	Yes	No	*a*, *b*, *c*	High	Variable	Yes	Yes	CHB based STATCOM
	[19]	Yes	Yes	*a*, *b*, *c*	Medium	Variable	Yes	Yes	
	[22], [23]	Yes	Yes	*α*, *β*	Medium	Variable	Yes	Yes	
	[24]	No	No	*α*, *β*	Medium	Variable	Yes	No	
M²PC	[25]	Yes	No	*a*, *b*, *c*	Medium	Variable	No	---------	MMC
	[26]	Yes	Yes	*a*, *b*, *c*	High	Variable	Yes	Yes	CHB based PET
	[27]	Yes	No	*a*, *b*, *c*	High	Variable	Yes	No	CHB BTB converter
	[28]	Yes	No	*a*, *b*, *c*	Medium	Variable	No	Yes	CHB based STATCOM
	[29]	Single-phase	No	---------	Medium	fixed	Yes	---------	MMC
	Proposed	**Yes**	**No**	***α*, *β***	**Low**	**Fixed**	**Yes**	**Yes**	CHB based STATCOM

TABLE II RUNTIME OF DIFFERENT BASIC OPERATIONS

Basic operations	Run cycles Ψ_{run}	Basic operations	Run cycles Ψ_{run}
Addition	1	Multiplication	1
Assignment	1	Absolute	2
Look-up	1	Comparison	1

TABLE III RUNTIME AND TIME COMPLEXITY OF MPC ALGORITHMS

MPC algorithms		Run cycles Ψ_{run}	Time complexity
Standard FCS-MPC [12]		$(30N + 10)(2^{N+1} - 1)^3$	$O(2^{3N})$
MPC with exhaustive search[15]		$264N^2 + 132N + 22$	$O(N^2)$
MPC for voltage balancing [18]		$90N\ (2^{N+1} - 1)$	$O(2^N)$
Polynomial fast MPC [19]		$96N^2 + 158N + 18$	$O(N^2)$
Proposed method	M²PC current control	492	$O(N)$
	cluster voltage balancing	$3N + 26$	
	individual voltage balancing	$6N + 6$	
	total	$9N + 533$	

$$\begin{bmatrix} P_{\alpha 0} \\ P_{\beta 0} \end{bmatrix} = \frac{V_0 I}{2} \begin{bmatrix} \cos(\varphi_i - \delta_0) \\ \sin(\varphi_i - \delta_0) \end{bmatrix} = \frac{1}{2} \begin{bmatrix} I_d & I_q \\ I_q & -I_d \end{bmatrix} \begin{bmatrix} V_0 \cos\delta_0 \\ V_0 \sin\delta_0 \end{bmatrix} \quad (15)$$

Based on (15), the final injected ZSV can be expressed as

$$\begin{bmatrix} V_0 \cos\delta_0 \\ V_0 \sin\delta_0 \end{bmatrix} = \frac{2}{-I_d{}^2 - I_q{}^2} \begin{bmatrix} -I_d & -I_q \\ -I_q & I_d \end{bmatrix} \begin{bmatrix} P_{\alpha 0} \\ P_{\beta 0} \end{bmatrix} \quad (16)$$

As shown in Fig. 3, the three-phase active power flow references are obtained by the PI controller on the differences between the rated DC capacitor voltage and the average value. Therefore, the cluster DC voltage balancing can be realized.

E. The modulation scheme

In this paper, the CPS-PWM is applied to realize the fixed switching frequency in each cell. With the input voltage three-phase output voltage references u_a^*, u_b^*, and u_c^*, these references are normalized to realize the comparisons with the carriers. It is noted that in order to realize accurate dynamic current prediction, the voltage references are divided by the real-time cluster DC voltages instead of the rated value NV_{dc}^*, which can be expressed as

$$n_j = \frac{u_j^*}{\sum_{m=1}^{m=N} V_{dcjm}}, \quad (j = a,b,c; m = 1,2,...,N) \quad (17)$$

where n_j is the modulation reference in each phase. The individual cell capacitor voltage balancing is realized by adjustments on the modulation references in each cell. With these adjustments, the final modulation reference is n_{jm}, which can be expressed as

$$n_{jm} = n_j + K_{pind}\ \mathrm{sgn}(i_j)(V_{dcjm} - \bar{V}_{dcjm}) \quad (18)$$

where the $\bar{V}_{dcjm}$ is the average value of the capacitor voltage in each phase, which can be expressed as

$$\bar{V}_{dcjm} = \sum_{m=1}^{m=N} V_{dcjm} / N, (j = a,b,c; m = 1,2,...,N) \quad (19)$$

Therefore, the individual capacitor voltage balancing can be realized.

F. Comparisons and computation complexity

To better elaborate the characteristics of the proposed M²PC method, a series of detailed comparisons with different MPC methods are listed in Table I.

For the MPC methods, most of them are designed for a three-phase CHB converter except the one in [17]. As for the weighting factors, the MPC method applied for inverters [14], and the multiple stages control method [18] requires no weighting factors. The proposed method eliminates the weighting factors by separated control between the current predictive control and the capacitor voltage balancing control. The proposed method is applied in the *α*-*β* coordinate, which requires less computation burden than those in the *abc* coordinate. Furthermore, this method reduces its computation burden by reduced evaluated control sets in each period. In terms of switching frequency, most of the existing MPC methods have no fixed switching frequency. Although an M²PC method is proposed in the CHB converter based PET system, it generates a fixed equivalent switching frequency for the output voltage levels instead of the cell switches. The proposed method can provide a fixed switching frequency for all the switches in each cell, which leads to a more balanced distribution of the switching loss. In addition, the delay

This article has been accepted for publication in a future issue of this journal, but has not been fully edited. Content may change prior to final publication. Citation information: DOI 10.1109/TIE.2021.3056953, IEEE Transactions on Industrial Electronics

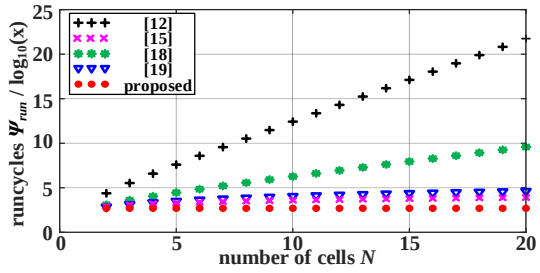

Fig. 7. The runtime of different MPC algorithms.

TABLE IV SYSTEM PARAMETERS

Items	Symbols	Simulations	Experiments
Grid line voltage	u_{gl}	10 kV	122 V
Grid Frequency	f_g	50 Hz	50 Hz
Rated DC capacitor voltage	V_{dc}^*	800 V	29 V
Filter inductance/resistor	L	10 mH	5 mH
	R	0.31 Ω	0.3 Ω
Carrier frequency	$f_{carrier}$	5 kHz	2 kHz
cell number per phase	N	12	4
SM capacitance	C	4 mF	3.84 mF

compensation of the proposed M^{2}PC method is also analyzed.

In order to better analyze the computation of the proposed method, a computation burden comparison with some MPC methods is further carried. According to reference [34], the complexity of the algorithms can be stated by the estimation of the required runtime. For the estimated real-time execution time, it can be expressed as

$$t_{real} = \psi_{run} T_{cycle} \tag{20}$$

where t_{real} is the estimated real-time of the controller; Ψ_{run} is the runtime of the algorithm; T_{cycle} is the execution time of the basic operation cycle.

Considering that different operations (such as addition, multiplication, absolute, and so on) require different runtimes, the required runtime for the common basic operations can be defined as in Table II. With the definition in Table II, the required runtime, and the complexity of the MPC algorithms are listed in Table III based on [19]. It is noted that for the proposed M2PC method, by properly designing the adaptive search step, only three evaluated control sets are necessary for each sampling period. Therefore, for the MPC algorithm, fixed run cycles are derived for each sampling period.

To vividly show the complexity of these algorithms, the runtime under different cell numbers are shown in Fig. 7, where N varies from 2 to 20. As shown in the figure, when the cell number N is higher than 1, the runtime of the proposed M2PC method is lower than other MPC methods.

IV. SIMULATION RESULTS

A three-phase CHB converter based STATCOM model is built in the MATLAB/ SIMULINK environment to verify the effectiveness of the proposed M^{2}PC method. The simulation parameters are selected as Table IV, according to reference [7].

A. Steady-state performance

The steady-state performance of the proposed M^{2}PC method is shown in Fig. 8, where the rated output current of CHB converter based STATCOM is set as 200 A. As is shown in Fig. 8 (a), the amplitude of the grid voltages is about 8165

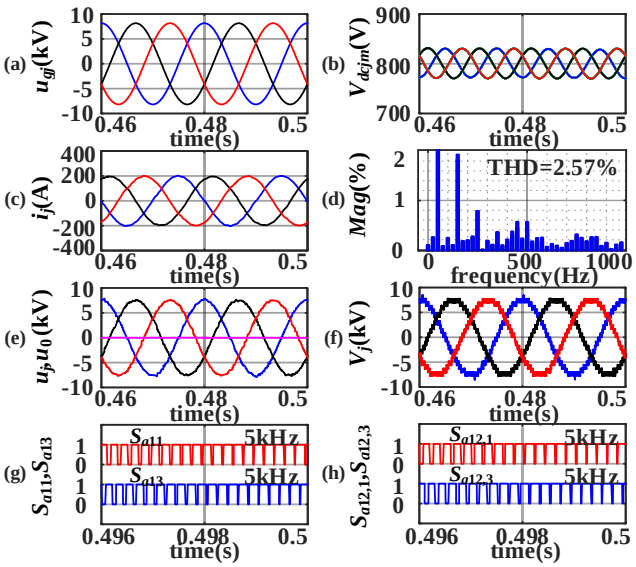

Fig. 8. Simulation steady-state performance of the proposed M^{2}PC method. (a) Grid voltages. (b) Capacitor voltages. (c) Output currents. (d) THD. (e) Output voltages references and the ZSV. (f) Output voltages. (g) Switching signals of S_{a11} and S_{a13}. (h) Switching signals of $S_{a12,1}$ and $S_{a12,3}$.

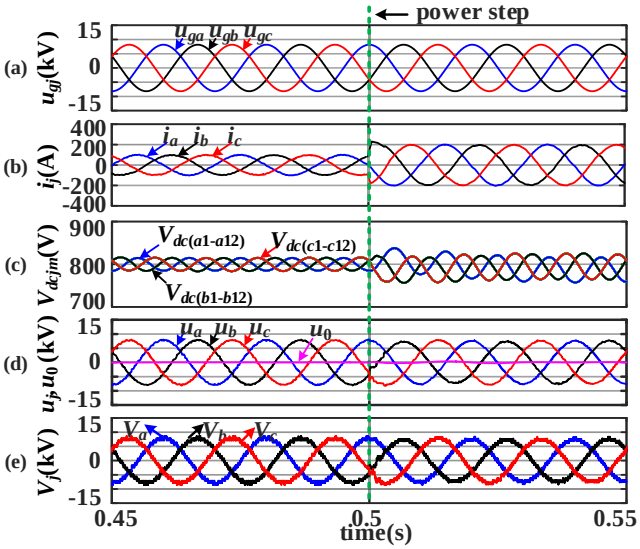

Fig. 9. Simulation dynamic performance of the proposed M^{2}PC method. (a) Grid voltages. (b) Output currents. (c) Capacitor voltages. (d) Output voltages references and the ZSV. (e) Output voltages.

V. The capacitor voltages are shown in Fig. 8 (b), where the average values remain stable at about 800 V. As shown in Fig. 8 (c), the amplitude of the output currents in CHB converter based STATCOM is 200 A, which is the same as the preset value. In addition, the phase angles of the current are 90 ° leading to the grid voltage, verifying the ability to generate reactive current. The current THD is about 3.65%, as shown in Fig. 8 (d). The output voltage references and the injected ZSV reference are shown in Fig. 8 (e), where the amplitude of the output voltage references are almost the same as that of the grid voltages. The injected ZSV is close to zero with the balanced cluster DC voltages. The three-phase output voltages are shown in Fig. 8 (f). The switching signals S_{a11} and S_{a13} in the first cell in phase A are shown in Fig 8 (g), and the switching signals $S_{a12,1}$ and $S_{a12,3}$ in the last cell in phase A are shown in Fig 8 (h). The switching frequencies of these switches are all 5 kHz, verifying the proposed method can

This article has been accepted for publication in a future issue of this journal, but has not been fully edited. Content may change prior to final publication. Citation information: DOI 10.1109/TIE.2021.3056953, IEEE Transactions on Industrial Electronics

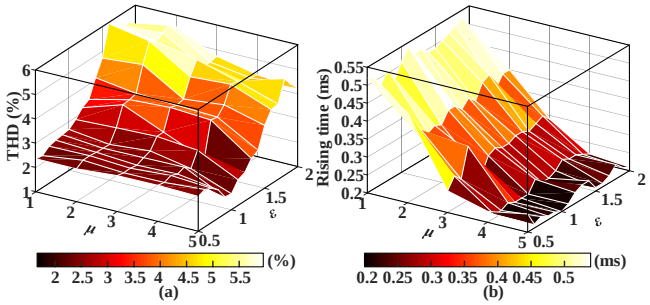

Fig. 10. The influence of μ and ε in the current predictive control on the performance of the proposed M^{2}PC method. (a). The influence of μ and ε on the output current (200 A) THD. (b). The influence of μ and ε on the rising time.

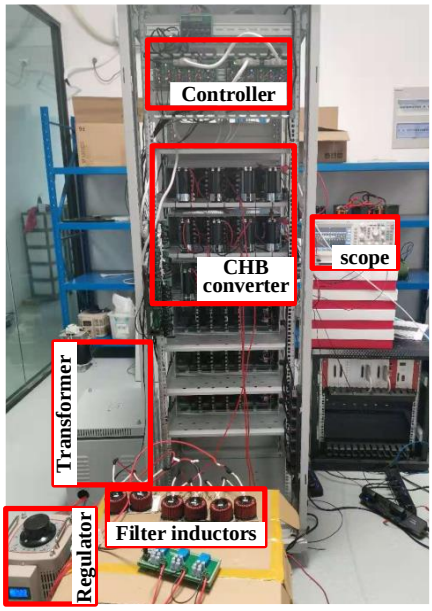

Fig. 11. The laboratory prototype of the three-phase down-scaled CHB converter based STATCOM.

generate a fixed switching frequency.

B. Power step performance

The dynamic response of the proposed method is shown in Fig. 9. In this scenario, the amplitude of the output currents in CHB based STATCOM increase from 100 A to 200 A at the time of about 0.5 s. As shown in Fig. 9 (a), the amplitude of the grid voltage is about 8165 V. As shown in Fig. 9 (b), the amplitude of the output currents increase from 100 A to 200 A at 0.5 s. The phase angles of the output currents are 90 ° leading to the grid voltage, generating reactive currents to the grid. The capacitor voltages are shown in Fig. 9 (c), the capacitor voltages remain stable at about 800 V. However, after the power step occurs, the capacitor voltage ripples increase slightly due to the increase of the output currents. The output voltage references and the injected ZSV are shown in Fig. 9 (d), where the amplitude of the output voltage references are almost the same as that of the grid voltages. The injected ZSV is close to zero due to the balanced cluster DC voltages. The output voltages in the three phases are shown in Fig. 9 (e). Simulation results verify that the proposed M^{2}PC method can operate normally and has a fast dynamic response during the power step operation.

C. Influence of search range and adaptive search step

To explore the influence of the search step and the

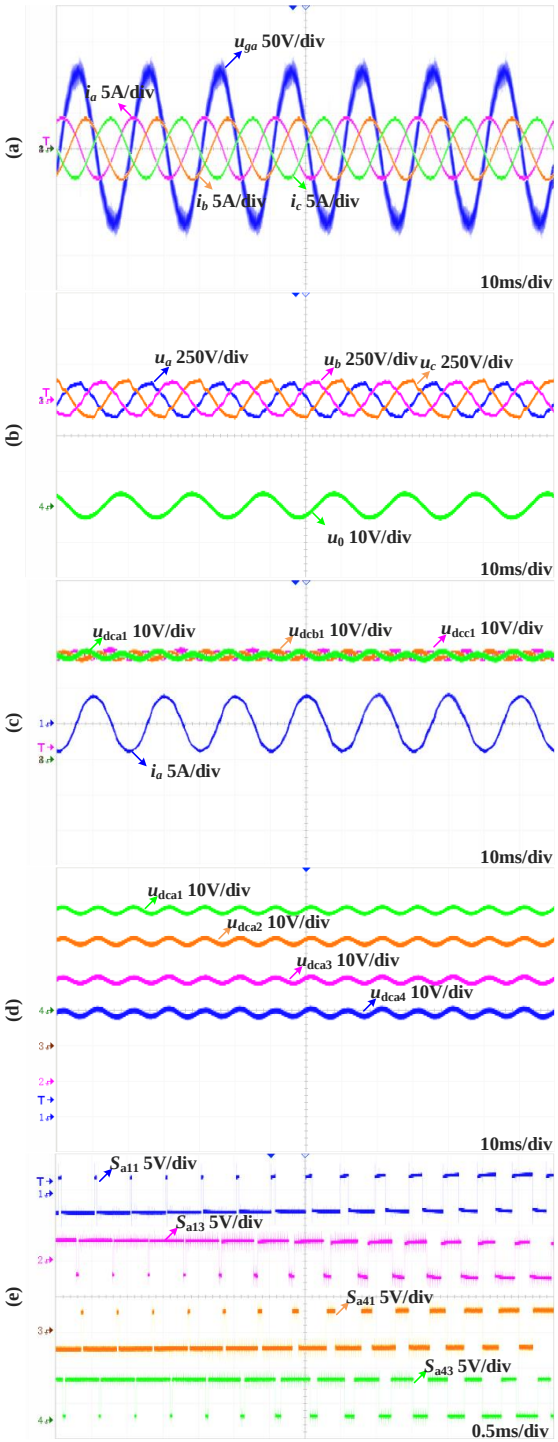

Fig. 12. Experimental steady performance of the proposed M^{2}PC method. (a) Grid voltages and output currents. (b) Output voltage references and injected ZSV references. (c) Output current and three-phase capacitor voltages. (d) Capacitor voltages in phase *A*. (e) Switching signals.

adaptive search range on the performance of the proposed M^{2}PC method, a series of simulations are conducted. Fig. 10 shows the influence on output current THD with an amplitude of 200 A, and the rising time with current amplitude rising from 100 A to 200 A. In Fig. 10, μ is the search range defined in equation (5), and ε is defined in equation (6). It is noted that since the output current is AC component, the rising time is calculated by the projection of the output currents on the *dq* axes. As shown in Fig. 10 (a), the search range μ has almost no influence on the output current THD. The output current

This article has been accepted for publication in a future issue of this journal, but has not been fully edited. Content may change prior to final publication. Citation information: DOI 10.1109/TIE.2021.3056953, IEEE Transactions on Industrial Electronics

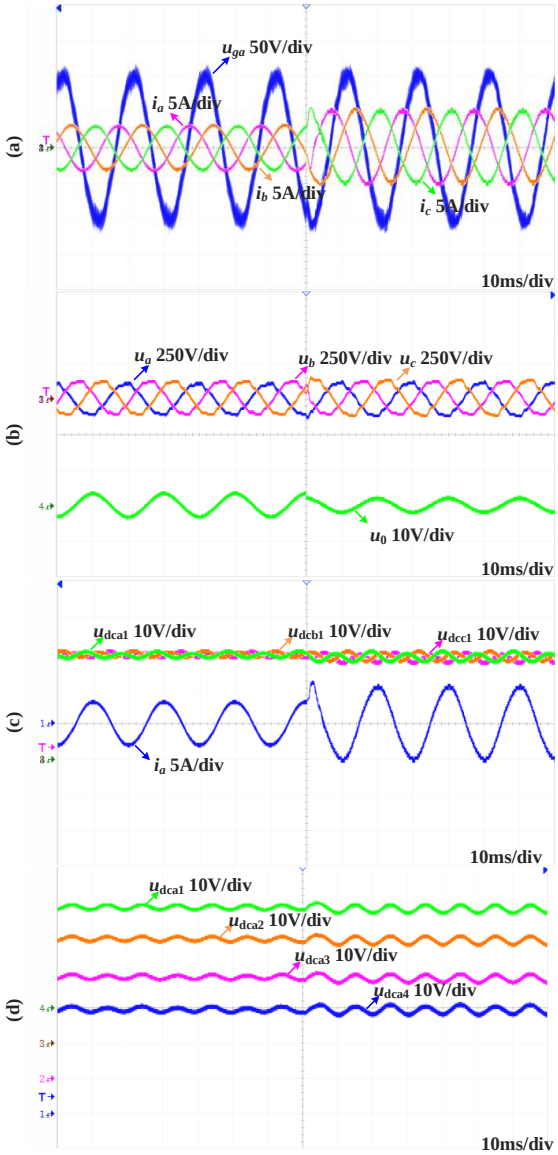

Fig. 13. Experimental power-step performance of the proposed M^{2}PC method. (a) Grid voltages and output currents. (b) Output voltage references and injected ZSV references. (c) Output current and three-phase capacitor voltages. (d) Capacitor voltages in phase *A*.

THD is mainly decided by the parameter for the adaptive search step ε. With the increase of ε from 0.5 to 2, the THD increases at the same time. As is shown in Fig. 10 (b), the parameter for the adaptive search step ε has almost no influence on the rising time. With the increase of μ from 1 to 5, the rising time decrease at the same time. The rising time in Fig. 10 (b) indicates that even the search range μ is selected as 1, the corresponding rising time is still tolerable and very low at about 0.5 ms. Therefore, with due consideration of the computation burden and the performance curve in Fig. 10, the final search range μ is selected as 1, and the parameter for the adaptive search step ε is selected as 1.

V. Experimental Results

In order to further verify the effectiveness and the dynamic response of the proposed method, experiments are conducted on a three-phase laboratory prototype. The prototype is shown in Fig. 11. The proposed control algorithm is implemented on the digital signal processing controller and the control signals from the controller are transferred to each cell by optical fiber. The output terminals of the converter are connected to the AC grid through filter inductors. The isolated transformer connected with a voltage regulator works as the AC grid. The oscilloscope is used to record the measured data. More detailed experimental parameters are also listed in Table IV.

A. Steady-state performance

The steady-state experimental performance of the proposed M^{2}PC method is shown in Fig. 12, where the rated output current of CHB converter based STATCOM is set as 4 A. In this experiment scenario, the output reactive current of the CHB converter based STATCOM is set to absorb inductive reactive current from the grid. As shown in Fig. 12 (a), the amplitude of the grid voltages is about 100 V, and the amplitude of the output currents in CHB converter based STATCOM is 4 A. In addition, the phase angles of the current are 90 ° leading to the grid voltage, verifying the ability to generate reactive current. The output voltage references and the injected ZSV reference are shown in Fig. 12 (b), where the amplitude of the output voltage references are almost the same as that of the grid voltages. The injected ZSV is about 5 V to balance the cluster DC voltages. The output current in phase A and the three-phase capacitor voltages are shown in Fig. 12 (c), where the three-phase DC capacitor voltages are well balanced at about 29 V, indicating the effectiveness of the DC cluster voltage balancing method. The individual capacitor voltages in phase *A* are shown in Fig. 12 (d), where the individual capacitor voltages are all stable at about 29 V, indicating the effectiveness of the individual capacitor voltage balancing method. The switching signals of the first cell and the last cell in phase *A* are shown in Fig 12 (e). It can be seen that for S_{a11}, S_{a13} in the first cell, and $S_{a4,1}$, $S_{a4,3}$ in the last cell, the switching frequency of each switch in each cell are fixed at about 2 kHz, verifying the fact that the proposed method can generate a fixed switching frequency.

B. Power step performance

The dynamic performance of the proposed M^{2}PC method is shown in Fig. 13. In this experiment scenario, the output reactive current of the CHB converter based STATCOM is set to absorb inductive reactive current from the grid. The amplitude of the reactive current rises from 3 A to 5 A. As shown in Fig. 13 (a), the amplitude of the grid voltages is about 100 V, which is in coherence with the preset input value. The output currents are also shown in Fig. 13 (a), where the amplitude of the output currents rise from 3 A to 5 A within 5 ms. In addition, the phase angle of output current remains at 90 ° leading to the grid voltage. Therefore, the fast dynamic response of the proposed modulated current predictive control is verified. The output voltage references and the injected ZSV reference are shown in Fig. 13 (b). Since the sampling frequency of the output references is the same as the carrier frequency, the voltage references are step signals changing at the frequency of about 2 kHz. Both the output voltage references and the ZSV references witness a step change during the power step so that the output currents can quickly and accurately track their references. The three-phase capacitor voltages and the output current in phase *A* are shown

in Fig. 13(c), where the average values of the capacitor voltage remain at about 29 V during the whole power step process. However, when the power step occurs, the voltage ripples of the capacitors increase slightly with the increase of the output current amplitude. The individual capacitor voltages in phase *A* are shown in Fig. 12 (d), where the average value of the individual capacitor voltages are all about 29 V, indicating the effectiveness of the individual capacitor voltage balancing method.

Experimental results verify that the proposed method obtains a good dynamic response, and it is able to generate a fixed switching frequency for the switches in each cell.

VI. Conclusion

In this paper, a novel M^{2}PC for CHB converter based STATCOM is proposed with a reduced computation burden and a fixed switching frequency in each cell. The proposed M^{2}PC method makes use of the adaptive search step for control sets under α-β coordinate, and a fixed reduced number of control sets are evaluated in each period. Therefore, the computation burden of the predictive control algorithm is fixed and reduced significantly. In addition, the cluster DC voltage balancing is realized by zero-sequence voltage (ZSV) injection, which does not influence the output current control in the α-β axes, and makes it possible to be applied in STATCOM operations. As a result, the cluster DC voltage balancing control is disintegrated with the output current predictive control, and the proposed M^{2}PC method requires no weight factors design process. Finally, with the effective combination of the proposed MPC control algorithm and the carrier phase shift (CPS) pulse width modulation (PWM), a fixed switching frequency in each cell can be obtained, which will be helpful for a more balanced distribution of the switching loss.

References

[1] X. Xing, X. Li, F. Gao, C. Qin, and C. Zhang. "Improved space vector modulation technique for neutral-point voltage oscillation and common mode voltage reduction in three-level inverter," *IEEE Trans. Power Electron.*, vol. 34, no. 9, pp. 8697-8714, Sep. 2019.

[2] H. Jia, Q. Xiao, and J. He, "An improved grid current and DC capacitor voltage balancing method for three-terminal hybrid AC/DC microgrid," *IEEE Trans. Smart Grid*, vol. 10, no. 6, pp. 5876-5888, Nov. 2019.

[3] L. Xiong, F. Zhuo, X. Liu, Z. Xu, and Y. Zhu, "Fault-tolerant control of CPS-PWM-based cascaded multilevel inverter with faulty units," *IEEE J. Emerg. Sel. Topics Power Electron.*, vol. 7, no. 4, pp. 2486-2497, Dec. 2019.

[4] Q. Xiao, L. Chen, Y. Jin, Y. Mu, A. F. Cupertino, H. Jia, Y. Neyshabouri, T. Dragicevic, and R. Teodorescu, "An improved fault-tolerant control scheme for cascaded H-bridge STATCOM with higher attainable balanced line-to-line voltages," *IEEE Trans. Ind. Electron.*, vol. 68, no. 4, pp. 2784-2797, Apr. 2021.

[5] Y. Neyshabouri, and H. Iman-Eini, "A new fault-tolerant strategy for a cascaded H-bridge based STATCOM, " *IEEE Trans. on Ind. Electron.*, vol. 65, no. 8, pp. 6436-6445, Aug. 2018.

[6] Q. Xiao, J. Wang, Y. Jin, L. Chen, H. Jia, T. Dragicevic, and R. Teodorescu. "A novel operation scheme for modular multilevel converter with enhanced ride-through capability of submodule faults," *IEEE J. Emerg. Sel. Topics Power Electron.*, online early access.

[7] R. Xu, Y. Yu, R. Yang, G. Wang, D. Xu, B. Li, and S. Sui, "A novel control method for transformerless H-bridge cascaded STATOM with star configuration," *IEEE Trans. Power Electron.*, vol. 30, no. 3, pp. 1189-1202, Mar. 2015.

[8] M Azab. "Performance of model predictive control approach for single-phase distributed energy grid integration with PQ control," *IET Energy Syst. Integr.*, vol. 1, no. 2, pp. 121–132, Jul. 2019.

[9] W. Chen, J. Yang, L. Guo, and S. Li, "Disturbance-observer-based control and related methods-An overview," *IEEE Trans. Ind. Electron.*, vol. 63, no. 2, pp. 1083-1095, Feb. 2016.

[10] Q. Xiao, L. Chen, H. Jia, P. Wheeler, and T. Dragicevic, "Model predictive control for dual-active-bridge in naval DC micro-grids supplying pulsed power loads featuring fast transition and online transformer current minimization," *IEEE Trans. Ind. Electron.*, vol. 67, no. 6, pp. 5197-5203, Jun. 2020.

[11] C. Zheng, T. Dragicevic, and F. Blaabjerg, "Current-sensorless finite-set model predictive control for LC-filtered voltage source inverters," *IEEE Trans. Power Electron.*, vol. 35, no. 1, pp. 1086-1095, Jan. 2020.

[12] P. Karamanakos, K. Pavlou, and S.Manias, "An enumeration-based model predictive control strategy for the cascaded H-bridge multilevel rectifier," *IEEE Trans. Ind. Electron.*, vol. 61, no. 7, pp. 3480-3489, Jul. 2014.

[13] J. Wang, X. Liu, Q. Xiao, D. Zhou, H Qiu, and Y. Tang, "Modulated model predictive control for modular multilevel converters with easy implementation and enhanced steady-state performance," *IEEE Trans. Power Electron.*, online early access.

[14] M. A. Perez, P. Cortes, and J. Rodriguez, "Predictive control algorithm technique for multilevel asymmetric cascaded H-bridge inverters," *IEEE Trans. Ind. Electron.*, vol. 55, no. 12, pp. 4354-4361, Dec. 2008.

[15] P. Cortes, A. Wilson, S. Kouro, J. Rodriguez, and H. Abu-Rub, "Model predictive control of multilevel cascaded H-bridge inverters," *IEEE Trans. Ind. Electron.*, vol. 57, no. 8, pp. 2691-2699, Aug. 2010.

[16] R. Baidya, R. Aguilera, P. Acuna, S. Vazquez, and H. D. Mouton, "Multistep model predictive control for cascaded H-bridge inverters: formulation and analysis," *IEEE Trans. Power Electron*., vol. 33, no. 1, pp. 876-886. Jan. 2018.

[17] C. Qi, X. Chen, P. Tu, and P. Wang, "Cell-by-cell-based finite-control-set model predictive control for a single-phase cascaded H-bridge rectifier," *IEEE Trans. Power Electron.*, vol. 33, no. 2, pp. 1654-1665, Feb. 2018.

[18] C. D. Townsend, T. J. Summers, and R. E. Betz, "Multigoal heuristic model predictive control technique applied to a cascaded H-bridge StatCom," *IEEE Trans. Power Electron.*, vol. 27, no. 3, pp. 1191-1200, Mar. 2012.

[19] Y. Zhang, X. Wu, X. Yuan, Y. Wang, and P. Dai, "Fast model predictive control for multilevel cascaded H-bridge STATCOM with polynomial computation time," *IEEE Trans. Ind. Electron.*, vol. 63, no. 8, pp. 5231-243, Aug. 2016.

[20] A. Dekka, B. Wu, V. Yaramasu, and N. R. Zargari, "Dual-stage model predictive control with improved harmonic performance for modular multilevel converter," *IEEE Trans. Ind. Electron.*, vol. 63, no. 10, pp. 6010-6019, Oct. 2016.

[21] J. Huang, B. Yang, F. Guo, Z. Wang, X. Tong, A. Zhang, and J. Xiao, "Priority sorting approach for modular multilevel converter based on simplified model predictive control," *IEEE Trans. Ind. Electron.*, vol. 65, no. 6, pp. 4819-4830, Jun. 2018.

[22] Y. Zhang, X.Wu, and X. Yuan, "A simplified branch and bound approach for model predictive control of multilevel cascaded H-bridge STATCOM," *IEEE Trans. Ind. Electron*., vol. 64, no. 10, pp. 7634-7644, Oct. 2017.

[23] Y. Zhang, X. Yuan, X. Wu, Y. Yuan, and J. Zhou, "Parallel Implementation of model predictive control for multilevel cascaded H-bridge STATCOM with linear complexity," *IEEE Trans. Ind. Electron*., vol. 67, no. 2, pp. 832-841, Feb. 2020.

[24] M. Nasiri, S. Farhangi, and J. Rodriguez, "Model predictive control of a multilevel CHB STATCOM in wind farm application using Diophantine equations," *IEEE Trans. Ind. Electron.*, vol. 66, no. 2, pp. 1213-1223, Feb. 2019.

[25] H. Mahmoudi, M. Aleenejad, and R. Ahmadi, "Modulated model predictive control of modular multilevel converters in VSC-HVDC systems," *IEEE Trans. Power Del.*, vol. 33, no. 5, pp. 2115-2124, Oct. 2018.

[26] L. Tarisciotti, P. Zanchetta, A. Watson, P. Wheeler, J. C. Clare, and S. Bifaretti, "Multiobjective modulated model predictive control for a multilevel solid-state transformer," *IEEE Trans. Ind. Appl.*, vol. 51, no. 5, pp. 4051-4060, Sep./Oct. 2015.

[27] L. Tarisciotti, P. E. Zanchetta, A. Watson, S. Bifaretti, and JC. Clare, "Modulated model predictive control for a seven-level cascaded h-

bridge back-to-back converter," *IEEE Trans. Ind. Electron.*, vol. 61, no. 10, pp. 5375-5383, Oct. 2014.

[28] L. Comparatore, J. Rodas, R. Gregor and M. Rivera, "Modulated model based predictive control with switcher of redundant states for a three-phase cascade H-bridge multilevel STATCOM," *2017 IEEE 18th Workshop on Control and Modeling for Power Electronics*, Stanford, CA, 2017, pp. 1-6.

[29] D. Zhou, S. Yang, and Y. Tang, "Model predictive current control of modular multilevel converters with phase-shifted pulse-width modulation," *IEEE Trans. Ind. Electron.*, vol. 66, no. 6, pp. 4368-4378, Jun. 2019.

[30] J. Gao, C. Gong, W. Li and J. Liu, "Novel compensation strategy for calculation delay of finite control set model predictive current control in PMSM," *IEEE Trans. Ind. Electron.*, vol. 67, no. 7, pp. 5816-5819, July 2020.

[31] X. Zhang, B. Hou, and Y. Mei, "Deadbeat predictive current control of permanent-magnet synchronous motors with stator current and disturbance observer," *IEEE Trans. Power Electron.*, vol. 32, no. 5, pp. 3818-3834, May 2017.

[32] Y. Yang, H. Wen, and D. Li, "A fast and fixed switching frequency model predictive control with delay compensation for three-phase inverters," *IEEE Acces*s, vol. 5, pp. 17904-17913, 2017.

[33] T. Jin, X. Shen, T. Su, and R. C. C. Flesch, "Model predictive voltage control based on finite control set with computation time delay compensation for PV systems," *IEEE Trans. Energy Convers.*, vol. 34, no. 1, pp. 330-338, Mar. 2019.

[34] X. Chen, J. Liu, S. Song, S. Ouyang, H. Wu, and Y. Yang, "Modified increased-level model predictive control methods with reduced computation load for modular multilevel converter," *IEEE Trans. Power Electron.*, vol. 34, no. 8, pp. 7310-7325, Aug. 2019.

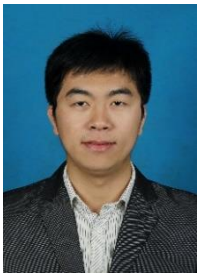

Qian Xiao received the B.S. and M.S. degrees in electrical engineering from Hebei University of Technology, Tianjin, China, in 2011 and 2014 respectively, and Ph.D. degree in electrical engineering from Tianjin University, Tianjin, China, in 2020. From Oct. 2018 to Nov. 2019, he was a visiting scholar with the Department of Energy Technology, Aalborg University, Aalborg, Denmark.

From Jan. 2020, he is currently an Assistant Professor with the School of Electrical and Information Engineering, Tianjin University. His research interests are multilevel converters, DC/DC converters, and power electronics for distributed generation, microgrids, and HVDC.

Yu Jin was born in Heilongjiang, China in 1994. He received B.S. from School of Electrical Engineering and Automation, Harbin Institute of Technology, Harbin 150001, China, in 2015. From October 2018 to October 2020, he was a visiting scholar with the Department of Energy Technology, Aalborg University, Aalborg, Denmark.

He is currently working for the Ph.D. degree in School of Electrical Engineering and Automation at Harbin Institute of Technology. His current research interests include multilevel converters and their applications in FACTS and multi-terminal microgrids, fault diagnosis and fault-tolerant control technique, and advanced control strategies in power converters.

Hongjie Jia received his Ph.D. degree in electrical engineering in 2001 from Tianjin University, China.

He became an Associate Professor at Tianjin University in 2002 and was promoted as Professor in 2006. His research interests include power reliability assessment, stability analysis and control, distribution network planning and automation, and smart grids.

Yunfei Mu (M'11) was born in Hebei, China. He received the Ph.D. degree from the School of Electrical Engineering and Automation, Tianjin University, Tianjin, China, in 2012. He is now a Professor with Tianjin University.

His research interests include integrated energy systems, electric vehicles, and smart grids.

Yanchao Ji (M'98) received the B.Eng. And M.Eng. degrees in electrical engineering from Northeast Electric Power University, Jilin, China, in 1983 and 1989, respectively, and the Ph.D. degree in electrical engineering from the North China Electric Power University, Beijing, China, in 1993.

He joined the Department of Electrical Engineering, Harbin Institute of Technology, Harbin, China in 1993. From 1995 to 1996, he was an Associate Professor with the Department of Electrical Engineering, Harbin Institute of Technology, where he is currently a Professor. His current research interests include pulse width modulation technique, power converter, and flexible ac transmission systems devices.

Remus Teodorescu (S'94–M'99–SM'02–F'12) received the Dipl.Ing. degree in electrical engineering from Polytechnical University of Bucharest, Romania in 1989, and PhD. degree in power electronics from University of Galati, Romania, in 1994.

In 1998, he joined Aalborg University, Department of Energy Technology, power electronics section where he currently works as a professor. He is a Fellow Member of IEEE. Between 2013 and 2017, he has been a Visiting Professor with Chalmers University. He was the coordinator of Vestas Power Program (2007 - 2013, involving 10 PhD projects in the areas of power electronics, power systems and energy storage. He has co-authored the book "Grid Converters for Photovoltaic and Wind Power Systems", ISBN-10: 0-470-05751-3 – Wiley and over 400 IEEE journals and conference papers. His areas of interests include: design and control of power converters for photovoltaics and wind power systems, grid integration with wind power, HVDC/FACTS based on MMC, SiC-based converters, and storage systems for utility.

Prof. Teodorescu was an Associate Editor of the IEEE Transactions on Power Electronics, and Chair of the IEEE Danish Joint IEEE Industrial Electronics Society, the IEEE Power Electronics Society, and the IEEE Industry Applications Society Chapter.

Frede Blaabjerg (S'86–M'88–SM'97–F'03) was with ABB-Scandia, Randers, Denmark, from 1987 to 1988. From 1988 to 1992, he got the PhD degree in Electrical Engineering at Aalborg University in 1995. He became an Assistant Professor in 1992, an Associate Professor in 1996, and a Full Professor of power electronics and drives in 1998. From 2017 he became a Villum Investigator. He is honoris causa at University Politehnica Timisoara (UPT), Romania and Tallinn Technical University (TTU) in Estonia.

His current research interests include power electronics and its applications such as in wind turbines, PV systems, reliability, harmonics and adjustable speed drives. He has published more than 600 journal papers in the fields of power electronics and its applications. He is the co-author of four monographs and editor of ten books in power electronics and its applications. He has received 33 IEEE Prize Paper Awards, the IEEE PELS Distinguished Service Award in 2009, the EPE-PEMC Council Award in 2010, the IEEE William E. Newell Power Electronics Award 2014, the Villum Kann Rasmussen Research Award 2014, the Global Energy Prize in 2019 and the 2020 IEEE Edison Medal. He was the Editor-in-Chief of the IEEE TRANSACTIONS ON POWER ELECTRONICS from 2006 to 2012. He has been Distinguished Lecturer for the IEEE Power Electronics Society from 2005 to 2007 and for the IEEE Industry Applications Society from 2010 to 2011 as well as 2017 to 2018. In 2019-2020 he served as a President of IEEE Power Electronics Society. He has been Vice-President of the Danish Academy of Technical Sciences.

He is nominated in 2014-2020 by Thomson Reuters to be between the most 250 cited researchers in Engineering in the world.